Soft Matter

Dynamic Article Links

Cite this: *Soft Matter*, 2011, **7**, 4111

www.rsc.org/softmatter

REVIEW

Internal motions of linear chains and spherical microgels in dilute solution

Zhuojun Dai,[a] To Ngai*[a] and Chi Wu[ab]

Received 10th November 2010, Accepted 15th January 2011
DOI: 10.1039/c0sm01291b

It is well known that for a flexible polymer chain in dilute solution, two different types of motions mainly contribute: the translation motion of the centres of mass of individual polymer chains; and the internal modes generated from the motions of segments with respect to the centre of mass of the chain. During the past two decades, with the advances in light scattering instrumentation and sophisticated methods of data analysis, both types of motions can be distinguished in experiments and utilized for testing molecular theories of polymer chain dynamics in dilute solution. In this article, we first review some previous experiments, in particular the dynamical properties of polystyrene (PS) and polyisoprene (PIP) chains in good and theta (Θ) solvents, and then our own results, including a comparative study of the internal motions of poly(*N*-isopropylacryl-amide) (PNIPAM) linear chains and spherical microgels under good solvent conditions. The final part of this article deals with how the solvent quality (the solution temperature) affects the internal mobility of PNIPAM linear chains and microgels.

1. Introduction

The dynamics of flexible polymer chains in dilute solution is an old and important problem in polymer physics.[1–6] When a polymer chain is flexible, it will not only move as one object but also change its conformation all the time to obtain its most probable distribution. These kinds of intrachain relaxations are referred to as internal motions, in contrast with the center-of-mass diffusion, which is also agitated by thermal energy.[7] In both free-draining and the non-draining models, internal motions of a polymer chain can be revolved into a series of normal modes with different frequencies.[1,2] It has been shown that these internal motions associated with the translational diffusion of flexible polymer chains in dilute solution will add additional broadening to the spectrum of the scattered light.[8] Theoretical predictions of the degree of this spectral broadening have been made on the basis of the bead-and-spring dynamical models with or without

[a]*Department of Chemistry, The Chinese University of Hong Kong, Shatin, N.T., Hong Kong*
[b]*The Hefei National Laboratory of Physical Science at Microscale, Department of Chem. Phys., The University of Science and Technology of China, Hefei, Anhui, 230026, China*

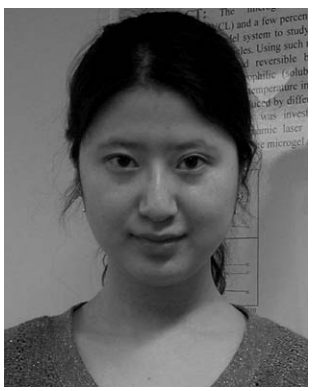

Zhuojun Dai

Zhuojun Dai was born in Xian, Shanxi province of China in 1987. She received her B.S. in polymer science and materials at Zhejiang University in 2005. Currently she is an M.Phil candidate in the Chemistry department of the Chinese University of Hong Kong under the supervision of Professor Chi Wu. Her research interests concentrate on the dynamics of polymer solutions and gel networks and development of non-viral vectors for molecular medicines.

To Ngai

To Ngai was born in the Fujian province of China in 1976. He received his B.Sc. degree in Chemistry from the Chinese University of Hong Kong in 1999. In 2003, he obtained his Ph.D. degree at the same university under the supervision of Professor Chi Wu. He moved to BASF (Ludwigshafen, Germany) in 2003; first as a post-doctoral fellow for one year, then as the chemist in the polymer physics division. He returned to Hong Kong in 2006 and has been an assistant professor since 2008. Currently, his research interests center on the designing, synthesizing and measuring interactions between polymers, particles and soft materials.

considering the hydrodynamic interactions.[3,8] Practically, dynamic laser light scattering (LLS) is a powerful technique, which detects not only the translational diffusion of the center of mass of individual polymer chains in solution but also their internal dynamics, provided that the average radius of gyration (R_g) is comparable or larger than the reciprocal of the scattering vector (q) or the wavelength of laser light used, where R_g ($= <R_g^2>^{z^{1/2}}$) is the root-mean square Z-average radius of gyration and $q = (4\pi n/\lambda_0)\sin(\theta/2)$ is the scattering vector with n, λ_0, and θ being the solvent refractive index, the wavelength in vacuum and scattering angles, respectively.[9–12]

The well-known Rouse-Zimm (RZ) model has been introduced to dynamic LLS analysis by a number of researchers, including Pecora,[3] and Dubois-Violette and de Gennes,[13] on the basis of the concept of dynamic structure factor, $S(q,t)$. In the region $qR_g \ll 1$, the contribution to $S(q,t)$ is mainly from the translational diffusion of the center of mass of the polymer chains. Therefore, $S(q,t)$ takes a single exponential form if polymer chains are monodisperse. On the other hand, when qR_g becomes larger than 1 and even for monodisperse polymer chains, $S(q,t)$ becomes multi-exponential owing to a visible contribution from a series of internal motions.[7] Due to the advancements of digital instruments and sophisticated data-analysis methods, these two types of relaxation processes can be experimentally distinguished and utilized to test related molecular theories of polymer chain dynamics in dilute solution.[14–16] Separation of internal motions and translational motions has been carried out by using the CONTIN method,[17] the double exponential or multiexponential fitting method,[18] the histogram method,[19] and the discrete inversion method.[20] The slowest mode is usually attributed to the translational motion whilst faster ones are assigned to internal relaxation modes which could be coupled to the translational motions.

In the past 40 years, the internal motions of various linear and flexible polymer chains in both good and Θ solvents have been systematically studied. For example, both static and dynamic properties of polystyrene (PS), a typical representative model of flexible chains, has been extensively studied in tetrahydrofuran (THF),[21–23] toluene,[24,25] benzene,[26–28] and ethylbenzene (ETBZ).[21] In recent years, armed with a new synthesis method,[29] flexible polymer chains with high molecular weight have been successfully prepared, which makes the study of the internal motions in the intermediate q region ($qR_g > 1$, but $ql < 1$) easier, where l is the length of a statistic segment. Besides PS, other flexible polymers or polymers with different conformations were chosen as model systems to qualitatively and quantitatively examine the internal motions.[30–32] Especially, we like to discuss the internal motions of a well-studied thermally sensitive polymer, poly(*N*-isopropylacrylamide) (PNIPAM).[33,34] Around its Θ temperature (~30.5 °C), the coil-to-globule transition of single chains and the volume transition of microgels occur when the solvent quality of water changes from good to poor as the solution temperature increases; namely, such a solution has a lower critical solution temperature (LCST). 15 years ago, we investigated the internal motions of PNIPAM linear chains and spherical microgels at lower temperatures (a good solvent condition).[35] Recently, we further studied how the solvent quality affects its internal motions by alternating the solution temperature from 25 °C to 40 °C.

In this review, we will first outline the theoretical background of the internal motions of polymer chains in dilute solution. After briefly summarizing some of previous works in old literature, we mainly focus on the results reported in the past 20 years.

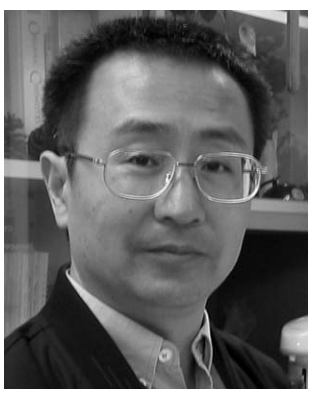

Chi Wu

Chi Wu was born in 1955 and graduated from USTC in Hefei, China in 1982. After obtaining his Ph.D. in 1987 followed by a two-year postdoctoral experience, under the supervision of Professor Benjamin Chu, in SUNY at Stony Brook, he moved to BASF, Germany in 1989; first as an Alexander von Humboldt Fellow and then as an employed researcher. He joined the Chinese University of Hong Kong in 1992 and is now Wei Lun Professor of Chemistry. His research combines synthetic chemistry, polymer physics and molecular biology to design and execute decisive experiments to answer questions in macromolecules, colloids and biology.

1.1 Theoretical background of internal motions

When a polymer chain is treated as a combination of springs and beads, its internal motions can be illustrated by how the motions of the beads change the lengths and orientations of the springs, which constantly reshape the chain conformation.[7] Both Rouse and Zimm deduced equations to describe this intrachain relaxation mode, separately in the draining and non-draining limits.[1,2] Although Zimm's consideration is much closer to the real situation, we still have to start with the deduction of the Rouse model since it is the simplest version of the bead-spring model and readily understood.

In the Rouse model, we assume that the chain has no excluded volume and there is no hydrodynamic interaction among different chains in the solution. In this model, the elastic forces on the nth bead ($n = 2, 3, \ldots, N-1$) are exerted by the two springs that connect their adjacent beads. At the same time, the nth bead receives a random force $\boldsymbol{f}_n$ from the solvent molecules. Supposing the spring force constant is $k_{sp} = 3k_BT/b^2$, and introducing $\boldsymbol{r}_0 = \boldsymbol{r}_1$ and $\boldsymbol{r}_{N+1} = \boldsymbol{r}_N$, where b is the spring length and $\boldsymbol{r}_i$ is the ith bead's position, we can write down the equation of motion for the nth bead as follows.

$$\zeta \frac{\mathrm{d}\mathbf{r}_n}{\mathrm{d}t} = k_{sp}(\mathbf{r}_{n-1} + \mathbf{r}_{n+1} - 2\mathbf{r}_n) + \mathbf{f}_n(t)(n = 1, 2...N) \qquad (1)$$

where ζ is the friction coefficient of each bead in the solvent. In eqn (1), the motions of each bead are correlated with others, which makes the exact solution of the equation rather difficult. To make the problem easier, normal coordinates are brought in, defined as

$$\mathbf{q}_i(t) = \frac{1}{N}\sum_{n=1}^{N} \cos\frac{in\pi}{N}\mathbf{r}_n(t) \ (i = 0, 1...) \qquad (2)$$

Here $\mathbf{q}_0(t)$ represents the global motion of the chain, namely, the translational diffusion. All the other normal modes correspond

to the internal motions. Furthermore, an inverse transformation leads to $\mathbf{r}_n$ as a combination of $\mathbf{q}_i$, *i.e.*,

$$\mathbf{r}_n(t) = 2\sum_{i=1}^{N-1}\cos\frac{in\pi}{N}\mathbf{q}_i(t) + \mathbf{q}_0(t) + (-1)^n\mathbf{q}_N(t)\ (n = 1, 2...N-1) \tag{3}$$

A combination of eqn (1) and (3) results in

$$\begin{aligned}\zeta\frac{\mathrm{d}\mathbf{q}_i}{\mathrm{d}t} &= \frac{1}{N}\sum_{n=1}^{N}\cos\frac{in\pi}{N}\zeta\frac{\mathrm{d}\mathbf{r}_n}{\mathrm{d}t}\\ &= \frac{1}{N}\sum_{n=1}^{N}\cos\frac{in\pi}{N}\mathbf{f}_n + k_{sp}\frac{1}{N}\sum_{n=1}^{N}\cos\frac{in\pi}{N}(\mathbf{r}_{n-1} + \mathbf{r}_{n+1} - 2\mathbf{r}_n) \quad (4)\\ &= \frac{1}{N}\sum_{n=1}^{N}\cos\frac{in\pi}{N}\mathbf{f}_n - k_{sp}\left(\frac{i\pi}{N}\right)^2\mathbf{q}_i\end{aligned}$$

where the friction coefficient ζ_i for ith mode is introduced for the convenience of later discussion. When $i = 0$, ζ_i equals to $N\zeta$ and in other case $2N\zeta$. Therefore, eqn (4) becomes

$$\zeta_i\frac{\mathrm{d}\mathbf{q}_i}{\mathrm{d}t} = -k_i\mathbf{q}_i + \mathbf{g}_i \tag{5}$$

with k_i and $\mathbf{g}_i$, respectively, presented as

$$k_i = k_{sp}\frac{\zeta_i}{\zeta}\left(\frac{i\pi}{N}\right)^2 = \frac{6\pi^2k_\mathrm{B}T}{Nb^2}i^2 \tag{6}$$

$$\mathbf{g}_i(t) = \frac{\zeta_i}{\zeta}\frac{1}{N}\sum_{n=1}^{N}\cos\frac{in\pi}{N}\mathbf{f}_n(t) \tag{7}$$

It clearly shows that the equation of motion for $\mathbf{q}_i$ depends on itself only, with the relaxation time τ_i defined as ζ_i/k_i

$$\frac{\mathrm{d}\mathbf{q}_i}{\mathrm{d}t} = -\frac{1}{\tau_i}\mathbf{q}_i + \frac{1}{\zeta_i}\mathbf{g}_i\ (i = 0,\ 1...) \tag{8}$$

While in the Zimm model, the hydrodynamic interactions among different beads are taken into account. In this case, the velocity of one bead affects all the other beads through the flow of solvent molecules. Zimm considered different hydrodynamic situations in both Θ and good solvents and derived the diffusion coefficient and relaxation time for each internal mode. In general, the longest intrachain relaxation time τ_1 can be expressed as

$$\tau_1 = M\eta_0[\eta]/A_1RT \tag{9}$$

where M is the molecular weight of the chain, $[\eta]$ and η_0 are the intrinsic and solvent viscosities, respectively, R is the gas constant, and T is the absolute temperature. The values of numerical factor A_1 are 0.822, 1.184 and 0.573, respectively, for the free-draining Rouse chain, the non-free-draining chain with and without pre-averaged hydrodynamic interaction.[36–38] In principle, the relaxation time of the pth mode can be calculated from the first mode by

$$\tau_p = \tau_1/p^\alpha \tag{10}$$

where the exponent $\alpha = 2.0$ and 1.5, respectively, for the free-draining (Rouse model) and non-draining models with the pre-averaged Oseen tensor. If the non-draining model is used without the pre-averaged Oseen tensor, the calculated relaxation times approximately increase by a factor of 2 in comparison with that obtained after the pre-averaging.[39] Later, both the Rouse and Zimm model were introduced into the theory of the quasi-elastic spectrum, which enables us to interpret those experimentally measured internal motions.

When a coherent and monochromatic laser beam hits a dilute solution of linear flexible polymer chains without any adsorption, the scattered light has a spectral distribution, $S(q,\omega)$, due to the translational diffusion and internal motions, as follows[40]

$$S(q,\omega) = (1/2\pi)\int e^{-i\omega t}e^{-q^2D|t|}S(q,t)dt \tag{11}$$

where ω is the angular frequency difference between the scattered and the incident light; D is the translational diffusion coefficient of individual chains; and $S(q,t)$ is generally expressed as

$$S(q,t) = \left\langle (1/N^2)\sum_{l=0}^{N}\sum_{m=0}^{N}e^{-i\mathbf{q}\cdot[\mathbf{r}_l(0) - \mathbf{r}_m(t)]}\right\rangle \tag{12}$$

due to interference of the scattered light from different segments within a long polymer chain made of N such segments, where $\mathbf{r}_l(0)$ is the position of the lth segment at time 0 and $\mathbf{r}_m(t)$ is the position of the mth segment at time t. The reference point is the center of mass of the chain. Therefore, all the spatial and temporal information related to intrachain, or called internal motions, is incorporated. Note that in a sufficiently diluted polymer solution, the interchain interference can be practically ignored. By incorporating the Oseen-Kirkwood-Riseman hydrodynamic interaction into the bead-and-spring model for a linear flexible polymer chain, Perico, Piaggio, and Cuniberti (PPC) have shown that the ensemble average in $S(q,\omega)$ is formulated as,[41,42]

$$\begin{aligned}S(q,\omega) = {} & P_0(x)L(w,q^2D) + \sum_{\alpha=1}^{N}P_1(x,\alpha)L(\omega,q^2D+\Gamma_\alpha) +\\ & \sum_{\alpha=1}^{N}\sum_{\beta=1}^{N}P_2(x,\alpha,\beta)L(\omega,q^2D+\Gamma_\alpha+\Gamma_\beta) +\\ & \sum_{\alpha=1}^{N}\sum_{\beta=1}^{N}\sum_{\gamma=1}^{N}P_3(x,\alpha,\beta,\gamma)L(\omega,q^2D+\Gamma_\alpha+\Gamma_\beta+\Gamma_\gamma) + \ldots\end{aligned} \tag{13}$$

where x is defined as $(qR_g)^2$, and $L(\omega,\Gamma)$ is a frequency ω-normalized Lorentzian distribution, centered at the frequency (ω_o) of the incident light, with Γ the line-width at the half-height; and P_n ($n = 0, 1, \ldots$), the intensity contribution of each Lorentzian to the line-width distribution $G(\Gamma)$. The zeroth-order $P_0(x)$ represents the contribution from the translational diffusion; $P_1(x,\alpha)$, the first-order contribution from the αth internal mode; $P_1(x,\alpha,\beta)$, the second-order contribution from both the αth and βth internal modes; and so on. At a relatively low scattering angle, *i.e.*, $x \ll 1$, the observation length ($1/q$) is much larger than the chain size so that each chain can be viewed as a point without any internal structure; namely, P_n ($n \geq 1$) diminishes and $S(q,\omega)$ only contains the first term. As x increases, $1/q$ gradually decreases so that the light begins to probe into segments of the chain, $P_n(n \geq 1)$ begins to contribute to $S(q,\omega)$ and the higher-order terms become more and more important.

In the study of the internal motions, the first cumulant $\Omega(q)$, defined as the initial slope of $S(q,t)$, is also an important parameter. As shown by de Gennes and Dubois-Violette on the basis of the Rouse-Zimm (RZ) spring-bead model, $\Omega(q)$ is q^2-dependent when $qR_g \ll 1$; and becomes q^3-dependent in an intermediate range of q.[43,44] As x further increases, the reduced first cumulant Ω^*, defined as $\Omega(q)/(k_BTq^3/\eta_0)$, gradually decreases and finally approaches a plateau value,[6,45,46] where η_0, k_B and T are the solvent viscosity, the Boltzmann constant and the absolute solution temperature, respectively.

1.2 Laser light scattering

In polymer and colloid science, laser light scattering is often referred to static (elastic) or dynamic (quasi-elastic) LLS. Static LLS as a classical and absolute analytical method measures the angular distribution of the excess absolute time-average scattered light intensity, known as the excess Rayleigh ratio $R_{vv}(\theta)$. At infinite dilution and the zero scattering angle ($\theta \rightarrow 0$), the weight-average molar mass (M_w) is related to $R_{vv}(\theta)$ by

$$\left[\frac{KC}{R_{vv}(\theta)}\right] \approx \frac{1}{M_w}\left(1+\frac{1}{3}<R_g^2>q^2\right) + 2A_2C \quad (14)$$

where $K = 4\pi^2n^2(dn/dC)^2/(N_A\lambda_0^4)$ with N_A is the Avogadro number, dn/dC is the specific refractive index increment, $<R_g^2>$ is the square average radius of gyration; and A_2 is the second virial coefficient. On the other hand, in dynamic LLS, we measure the intensity fluctuation of the scattered light. Since the internal motions are mainly studied by dynamic LLS so that we detail its quasi-elastic nature as follows.

When the incident light is scattered by moving macromolecules or particles, the detected frequency of the scattered light will be slightly higher or lower than that of the incident light owing to the well-known Doppler effect, depending on whether the particle moves towards or away from the detector. Therefore, the resultant frequency distribution of the scattered light is slightly broader than that of the incident light. Quantitatively, the incident light has a frequency of $\sim 10^{15}$ Hz; while the broadening is only $\sim 10^5$–10^7 Hz, depending on how fast the scattering objects move inside the solution. Therefore, it is very difficult to directly detect such a small broadening ($\sim 10^6/10^{15}$) in the frequency domain. However, it can be effectively recorded in the time domain through a time autocorrelation function, $G^{(2)}(q,t)$, *i.e.*, the intensity-intensity time correlation function, defined as $<I(q,0)I(q,t)>/<I(q)>^2$ in the self-beating or homodyne mode, where t is the delay time and $<I(q)>$ is the time-average scattering intensity. Each measured $G^{(2)}(q,t)$ can be related to a normalized electric field-field time correlation function $g^{(1)}(q,t)$ by the Siegert relation as

$$G^{(2)}(q,t) = A[1 + B\,|g^{(1)}(q,t)|^2] \quad (15)$$

where A is a baseline; $0 \leq B \leq 1$, a spatial coherent constant depending only on the instrumental detection optics. The value of B actually reflects the signal-to-noise ratio of a dynamic light-scattering experiment. $g^{(1)}(q,t)$ is proportional to $S(q,t)$ and related to the characteristic line-width distribution $G(\Gamma)$ by

$$g^{(1)}(q,t) = \int_0^\infty G(\Gamma)e^{-\Gamma t}d\Gamma \quad (16)$$

where $G(\Gamma)d\Gamma$ is the statistic (intensity) weight of the scattering objects (particles or macromolecules) which possess a line-width Γ. For a dilute solution, Γ measured at a finite scattering angle is related to C and q by:

$$\Gamma = q^2D(1 + k_dC)(1 + fq^2 < R_g^2 > z) \quad (17)$$

where D is the translational diffusion coefficient of the solute molecule at $C \rightarrow 0$, k_d is the diffusion second viral coefficient, and f is a dimensionless parameter depending on polymer chain structure and solvent (for polymers with flexible chains in a good solvent, f is between 0.1 and 0.2). Therefore, when $C \ll 1$ and $qR_g < 1$, $D \simeq \Gamma/q^2$. In other words, for narrowly distributed polymer chains or spherical colloidal particles in a dilute solution or dispersion at $x \ll 1$, $G(\Gamma)$ can be converted into a pure translational diffusion coefficient distribution $G(D)$ by $D = \Gamma/q^2$ or further to a hydrodynamic radius distribution $f(R_h)$ by using the Stokes-Einstein equation.

$$R_h = \frac{k_BT}{6\pi D\eta_S} \quad (18)$$

However, as the scattering angle increases, *i.e.*, when $1/q$ is comparable to the size of a flexible scattering object, one has to consider the internal relaxation processes because light probes the motions inside these larger "particles" and their contributions to $G(\Gamma)$ become more and more important. The coexistence of the translational relaxation and internal motions can be analyzed by the following double exponential equation.

$$\left|g^{(1)}(\tau)\right| = A_D\exp(-\Gamma_D\tau) + A_I\exp(-\Gamma_I\tau) \quad (19)$$

where A and Γ are the intensity weighting and the characteristic delay rate of the relaxation, respectively; subscripts "D" and "I" denote the diffusion and internal modes. Note that $A_D + A_I = 1$. This fitting enables us to obtain few characteristic parameters related to the internal motions, including the longest relaxation time and the first cumulant. For monodispersed polymer chains at infinite dilution, $g^{(1)}(\tau)$ is theoretically expressed as

$$|g^{(1)}(\tau)| = P_0(x)\exp(-q^2D_0\tau) + P_1(x)\exp[-(q^2D_0 + 2\tau_1^{-1})\tau] + \ldots \quad (20)$$

where D_0 is the translational diffusion coefficient, τ_1 is the longest intrachain relaxation time, and the expansion coefficients $P_i(x)$ obeys

$$P(x) = P_0(x) + P_1(x) + \ldots = (2/x^2)(e^{-x} - 1 + x) \quad (21)$$

A combination of them with the double exponential analysis leads to the following equation with a collective intrachain relaxation time τ_c.

$$|g^{(1)}\tau)| = A_D\exp(-q^2D\tau) + A_I\exp[-(q^2D + 2\tau_c^{-1})\tau] \quad (22)$$

A comparison of eqn (19) and (22) shows that

$$\Gamma_D = Dq^2 \quad (23)$$

$$\Gamma_I - \Gamma_D = 2/\tau_c \quad (24)$$

It is clear that τ_c contains the contributions from all the internal modes and becomes τ_1 only when qR_g approaches zero. On the other hand, the first cumulant can be calculated on the basis of the double exponential method. The first cumulant is defined as[47]

$$\begin{aligned}\Omega &= -\lim_{\tau\to 0} d\left|g^{(1)}(\tau)\right|/\mathrm{d}\tau \\ &= \lim_{\tau\to 0}\int_0^\infty \Gamma G(\Gamma)\exp(-\Gamma\tau)\mathrm{d}\Gamma = \Gamma_e\end{aligned} \tag{25}$$

Γ_e is named as the effective decay rate, identical to the first cumulant. Using eqn (19), we have

$$\Omega = \Gamma_e = A_D\Gamma_D + A_I\Gamma_I \tag{26}$$

In our laboratory, a modified commercial LLS spectrometer (ALV/DLS/SLS-5022F) equipped with a multi-τ digital time correlator (ALV5000) and a cylindrical 22 mW UNIPHASE He-Ne laser ($\lambda_0 = 632$ nm) was used. The incident beam was vertically polarized with respect to the scattering plane and the intensity was regulated with a beam attenuator (Newport M-925B) so that possible localized heating in the light scattering cuvette is avoided. Note that the highest reachable scattering angle in LLS spectrometers is practically limited to 160°.

2. Discussion

The dynamics of linear flexible chains in dilute solutions have been studied extensively. Previous experimental data have been accumulated mainly for polystyrene (PS) because it has long been considered as a good model polymer of linear flexible chains. Later on, other flexible polymers, such as polyisoprene (PIP) and poly(*N*-isopropylacrylamide) (PNIPAM) were used. In the following discussion, we first review the dynamical properties of PS and PIP chains in good and Θ solvents, and then turn to our recent studies. In particular, the internal motions for PNIPAM chains and spherical microgels at both good and Θ solvents will be discussed.

2.1 Internal motions of PS chains in dilute solution

The theoretical basis for interpreting dynamic LLS in dilute polymer solution was given by Pecora, who showed that the spectrum of the scattered light should consist of a pure translational diffusion as well as intramolecular relaxations. The intensity weighting of the diffusive mode to the total scattered intensity was predicted to depend uniquely on the parameter x which equals $(qR_g)^2$. As shown and discussed in eqn (13), for $qR_g \ll 1$, only the pure translational mode contributes to the $S(q,t)$. However, in an intermediate range of qR_g, $S(q,t)$ is composed of contributions from both translational diffusion and internal motions. Following these theoretical considerations, previous experimental studies were focused on interpretation of the $S(q,t)$ in the intermediate qR_g region by appropriate extrapolation to infinite dilution and zero scattering angle in order to obtain a value of τ_1, which is associated with the first mode or the longest intrachain relaxation time of a given polymer solvent system. The applied methods of analysis included double exponential fits, histogram analysis, CONTIN,[17] and MAXENT.[48] For earlier experiments of PS in methyl ethylketone (marginal solvent) and cyclohexane (Θ solvent),[49,11] the obtained τ_1 values were in agreement with values estimated from the free-draining Rouse model. However, later studies on the same systems yielded τ_1 values in agreement with the non-draining Zimm prediction.[50–52] The conflicting results were attributed to the fact that none of these initial studies were performed over a wide range of concentrations and scattering angles, which facilitates appropriate comparison of theory and experiment. Tsunashima and coworkers[45,46] have investigated dynamics of dilute solutions of narrow-distribution PS in *trans*-decahydronaphthalene at the Θ temperature, and in good solvents, *trans*-decalin as well as benzene over a wide range of qR_g by means of dynamic LLS. They found that the deduced τ_1 values, in each case, to be quantitatively described by non-draining Zimm model. However, the contribution of the translation diffusion motion relative to that of all molecular motions showed substantial differences in good and Θ solvent systems because of the varied strengths of the hydrodynamic interactions. Bhatt and Jamieson[53] have investigated the dynamic LLS properties of dilute solutions of narrow distribution PS in tetrahydrofuran (THF) and ethlybenzene (ETBZ) at 25 °C in the range $1 < qR_g < 6$. The τ_1 values for PS in THF were similar to the values predicted by a non-draining Gaussian chain model with preaveraged Oseen hydrodynamic interaction, but data for the good solvent, ETBZ, were not consistent with this theory. On the other hand, the τ_1 values for PS in ETBZ, corrected for solvent viscosity, were approximately 50% larger than those obtained in THF. This observation suggests inherent differences in the nature of the internal chain dynamics in these two good solvent systems; namely, there is a larger draining effect in the PS/ETBZ system. The decrease in solvent draining in PS/THF was thus predicted to lead to an enhanced contribution from internal motions.

Chu and coworkers[54] have also presented an investigation of internal motions of PS in benzene from the measured intensity time correlation function by using a combination of a specially designed low-angle LLS spectrometer with a prism cell and a conventional wide-angle LLS spectrometer. They demonstrated that, in addition to the longest internal relaxation time τ_1, the second internal motion τ_2 could also be determined under appropriate conditions. According to the existing theories for a flexible polymer chain under both the free-draining and non-draining limits, Perico *et al.*[41] showed at $x > 1$, $S(q,t)$ is dominated by the first five relaxation processes, namely, a pure translational diffusion term plus four principle internal motions. Therefore, at $x > 1$, eqn (13) in the time domain can be rewritten as

$$\begin{aligned}S(q,t) = P_0(\mathrm{x})e^{-Dq^2t} + P_1(x,1,1)e^{-(Dq^2+2\Gamma_1)t} + \\ P_2(x,2)e^{-(Dq^2+\Gamma_2)t} + P_3(x,1,1,1,1)e^{-(Dq^2+4\Gamma_1)t} + \\ P_4(x,2,2)e^{-(Dq^2+2\Gamma_2)t} + \ldots\end{aligned} \tag{27}$$

where the numeric values of P_n in the range of $1 \le x \le 10$ have been calculated by PPC. Using Zimm model, we have

$$\Gamma_n = \frac{0.293RT\lambda_n'}{M[\eta]\eta_0} \tag{28}$$

where $[\eta]$ and λ_n' are the intrinsic viscosity and the eigenvalues, respectively. Normalized by Dq^2 and converting q to x, we can rewrite eqn (28) as

$$\Gamma_n/(Dq^2) = \frac{0.293\lambda_n' RTR_g^2}{M[\eta]D\eta_0 x^2} \quad (29)$$

Therefore, $\Gamma_n/(Dq^2)$ can be calculated from eqn (29) with the known values of D, M, R_g, λ_n', η_0, and $[\eta]$. By using the numeric values of P_n reported by Perico *et al.*[41] and the values of Γ_n calculated from eqn (29), we are able to calculate the average line width $<\Gamma>_{int}$ associated with the internal motions, *i.e.*,

$$<\Gamma>_{int} = [\sum_{\alpha=1}^{N} P_1(x,\alpha)(Dq^2+\Gamma_\alpha)+ \sum_{\alpha=1}^{N}\sum_{\beta=1}^{N} P_2(x,\alpha,\beta)(Dq^2+\Gamma_\alpha+\Gamma_\beta)+...]/[\sum_{\alpha=1}^{N} P_1(x,\alpha)+ \sum_{\alpha=1}^{N}\sum_{\beta=1}^{N} P_2(x,\alpha,\beta)+...] \quad (30)$$

Experimentally, Chu *et al.*[54] successfully observed the first two internal relaxation times, τ_1 and τ_2, at proper regimes of $1 < x < 3$, and $3 < x < 6$ respectively, for polymer chain at the non-free-draining limit. One therefore may wonder that higher order internal motions, such as τ_3, τ_4, and so on could also be detected as x increases beyond the x range reported by them.

Some experiments by our group cast new light on this problem.[55] The $S(q,t)$ from three high molecular weight PS polymers (HPS-1, $M_w = 6.33 \times 10^6$ g mol^{-1}; HPS-2, $M_w = 9.80 \times 10^6$ g mol^{-1}; HPS-3, $M_w = 16.4 \times 10^6$ g mol^{-1}) in dilute toluene solution were precisely studied by dynamic LLS over a wide range of scattering angles (6–154°). Fig. 1 shows typical plots of $G(\Gamma/q^2)$ *versus* Γ/q^2 for HPS-2 in toluene at different x values; the insert shows a ~10 times enlargement of the second (smaller) peak of the distribution in the range of 10^{-7}–10^{-6} cm^2/s. At $x < 1$, as expected and discussed above, only one single and narrow peak related to translational diffusion was observed. At $x \sim 1$, a second peak with a higher Γ appears in $G(\Gamma/q^2)$, while the first peak is basically unchanged in position and shape. This second peak is related to the internal motions. At $x > 1$, the first peak is getting broader and shifting to higher Γ. This is because at higher x our LLS probe scale (q^{-1}) is smaller than the chain dimension ($\sim R_g$), so that the contribution from the translational and internal motions are mixed in the measured spectrum which resulted the broadening and shifting of the first peak. At $x > 15$, the first and second peaks in $G(\Gamma/q^2)$ merge into a single and broader distribution. This can be explained by the fact that the line width (Dq^2) associated with the pure translational diffusion increases with x, but the line widths related to the internal motions are independent of the scattering angle.

Fig.2 shows a plot of this $\Gamma_{peak2}/(Dq^2)$ against x for HPS-1(○), HPS-2(□), and HPS-3(△) in toluene at 20 °C, where Γ_{peak2} is the average line width of the second peak in Fig. 1. For comparison, the experimental data from Chu *et al.*[54] (filled diamonds) and Kurata *et al.*[46] (filled circles) were also plotted in Fig. 2. Clearly, these data were in agreement with ours in the comparable x values. According to the PPC's theory and if eqn (27) is right, Γ_{peak2}/Dq^2 calculated from the second peak of the line-width distribution in Fig. 1 should follow the line of $<\Gamma>_{peak2}/Dq^2$ *versus* x. However, the plot of $<\Gamma>_{peak2}/Dq^2$ *versus* (the solid line) in Fig. 2 shows a clear deviation between the experimental data and the calculation. On the other hand, Fig. 2 shows that the experimental data have a tendency to respectively follow the dotted lines of $n = 1$ in $1 < x < 3$; $n = 2$ in $3 < x < 6$; $n = 3$ in $6 < x < 10$; and $n = 4$ in $10 < x < 15$. In other words, by analyzing the Γ_{peak2}/Dq^2 in Fig. 2 with an assumption of $\Gamma_{peak2}/Dq^2 = 1 + 2\Gamma_n/(Dq^2)$, we were able to determine Γ_1, Γ_2, Γ_3, Γ_4 in different ranges of x. For $x > 15$, the two peaks in Fig. 1 merge into one, which makes it difficult for us to get a precise Γ_{peak2} value from the spectral distribution so that we stop our second-peak analysis of these high x value data in order to avoid any ambiguity. Furthermore, both Chu's and our experimental data clearly indicated that the internal motions associated with $2\Gamma_n$, *i.e.*, $\Gamma_n + \Gamma_n$, dominate the relaxation process in different ranges of x, where n is the order of the internal motion. On the basis of eqn (13) and (27), this ($\Gamma_n + \Gamma_n$) relaxation implies a self-coupling of the nth-order internal motion. We have no explanation why only these kind of self-coupled internal motions were observed in dynamic LLS. According to eqn (13), energetically, it is easier to excite the internal motions associated with Γ_1 and $4\Gamma_1$ than that associated with $2\Gamma_2$. The fact that we observed $2\Gamma_2$ instead of Γ_1 and $4\Gamma_1$ in the range of $3 < x < 6$ might suggest that the ability of

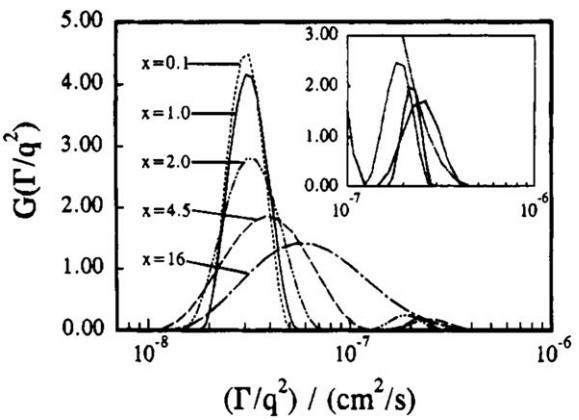

Fig. 1 Typical plot of $G(\Gamma/q^2)$ *versus* Γ/q^2 for HPS-2 in toluene at 20 °C and different x values wherein the inset shows a ×10 enlargement of the second peak of the distribution in the range of 10^{-7} – 10^{-6} cm^2/s. Reprinted with permission from ref. 55, (1995 American Chemical Society).

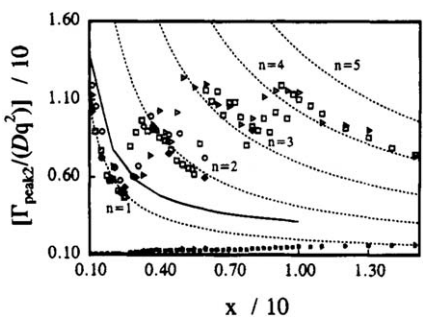

Fig. 2 Plot of $\Gamma_{peak2}/(Dq^2)$ *versus* x for HPS-1(○), HPS-2(□), and HPS-3(△) in toluene at 20 °C where Γ_{peak2} is denoted the average line width of the second peak. For comparison, we included the experimental data from Chu *et al.* (filled diamonds) and Kurata *et al.* (filled circles). Reprinted with permission from ref. 55 (1995 American Chemical Society).

dynamic LLS to measure a certain kind of internal motion may be related to the observation length scale, $1/q$. In other words, even though some energetically favorable internal motions exist, we cannot "see" them in a certain range of x.

Akcasu *et al.*[37] have developed another method for the interpretation of dynamic LLS experiments over the entire accessible q range in terms of the first cumulant $\Omega(q)$ of $S(q,t)$ which is the initial slope of $S(q,t)$ and can be determined by the cumulant analysis of $S(q,t)$. The advantage is that this method is quite useful for the test of various molecular modes which accounted for the hydrodynamic interaction as well as the exclude volume effect. Han and Akcasu have presented a systematic study in which they explored the q dependence of the $\Omega(q)$ as a function of PS molecular weight (from 10^6 to 10^7 g mol^{-1}) in both good and Θ solvents, and compared their results to the theoretical predictions.[6] It was found that $\Omega(q)$ approaches q^2 dependence for $qR_g \ll 1$ and q^3 dependence for $qR_g \gg 1$, with a broad transition region. As qR_g further increased, the reduced first cumulant Ω^*, defined as $\Omega(q)/(k_BTq^3/\eta_0)$, gradually decreased and finally approached a plateau value, where k_B is the Boltzmann constant. This universal scaling of Ω^* with q^3 is consistent with the non-free-draining bead-and-spring model for flexible polymer chains in infinite dilute solution. On the basis of PS in Θ solvent cyclohexane, however, Han and Akcasu have reported $\Omega^* \cong 0.045$, which was about 18% smaller than the theoretical prediction; namely, 0.071 with preaveraged Oseen tensor and 0.079 without a preaveraged Ossen tensor.

Nemoto *et al.* pointed out that for precisely testing the theories, it is necessary to extrapolate the $\Omega(q)$ to infinite dilution and zero scattering angle.[46] After this treatment, for PS in the good solvent, benzene, the obtained Ω^* vaules were still 25% smaller than the theoretical estimates. When it comes to PS in Θ solvent, *trans*-decahydronaphthalene, the difference between the experimental value and the theoretical value reduced to about 15%. They speculated that the established theory may overestimate the amplitude of the internal modes, since theoretical prediction assumed complete flexibility to the swollen polymer chains, while the intramolecular relaxation are more or less depressed in a swollen chains even in a good solvent. Fig. 3 shows our data in a typical plot of the $\Omega(q)/(k_BTq^3/\eta_0)$ *versus* $x^{1/2}$ for PS in toluene at 20 °C. The plateau value of $\Omega(q)/(k_BTq^3/\eta_0)$ is around 0.05. This consistent lower plateau value shows that, at larger x, there exist some problems in the theoretically predicted $G(\Gamma)$. For the study of PS in good solvent, THF, Bhatt and Jamieson yielded $\Omega^* \cong 0.061$, closer to the theoretical prediction.[56] To rationalize the discrepancy, they suggested the revision of the classical theory by including phenomena such as internal friction, chain rigidity, variations in the degree of draining, and hydrodynamic screening.

2.2 Internal motions of PIP chains in dilute solution

In the late 1980s, Tsunashima *et al.* suggested using rubbery polyisoprene (PIP) to study the dynamic properties of polymer chains in dilute solution.[57] They speculated that some parts of the discrepancies between the experimental results and theoretical predictions might derive from insufficient chain flexibility in PS polymer. It has been found that PIP chains are fairly well represented by the non-draining Gaussian chain model with nonpreaveraged Oseen hydrodynamic interaction.[43] However, for PIP in Θ solvent 1,4-dioxanea value of $\Omega^* \cong 0.048$ has been obtained, which is 20% smaller than the predicted value for a Θ system. The authors speculated about the reason for the deviation due to the incompleteness of the theory. For PIP in cyclohexane, a good solvent, they deduced $\Omega^* \cong 0.06$, larger than that observed for PS, which was surprisingly in agreement with the Akcasu-Gurol prediction for non-draining Gaussian chains using non-preaveraged hydrodynamic interactions. Their results partially confirmed that the source of deviations between prediction and experiment for PS lies in its comparative conformational rigidity.

2.3 Internal motions of PNIPAM chains in dilute solution

Poly(*N*-isopropylacrylamide) (PNIPAM) is a temperature sensitive polymer with a lower critical solution temperature (LCST) at about 32 °C. Below LCST, water is its good solvent due to the hydrogen bond formed between the polymer and water molecule. However, with the increasing temperature, the hydrogen bond is destroyed and the water changes from a good solvent to Θ solvent and finally a bad solvent. During this process, the PNIPAM chain will exhibit a swollen to shrunk transition within a very narrow temperature range. In this section, we will first examine the properties and change of internal motion of PNIPAM chains in dilute solution under the good solvent conditions.

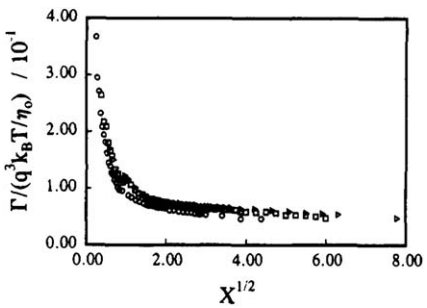

Fig. 3 Plot of $\Omega(q)/(k_BTq^3/\eta_0)$ *versus* $x^{1/2}$ for HPS-1(○), HPS-2(□), and HPS-3(△) in toluene at 20 °C, where T is the absolute temperature, and k_B, the Boltzmann constant. Reprinted with permission from ref. 55 (1995 American Chemical Society).

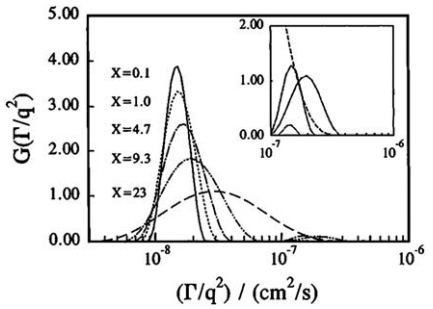

Fig. 4 Typical line-width distributions $G(\Gamma/q^2)$ of the PNIPAM linear chains at $T = 15.0$ °C. The insert shows a tenfold enlargement of the second peak in the range of $10^{-7} < \Gamma/q^2 < 10^{-6}$ cm^2/s. Reprinted with permission from ref. 35, (1995 American Chemical Society).

Fig. 4 shows typical plots of the line-width distributions $G(\Gamma/q^2)$ *versus* Γ/q^2 for individual PNIPAM linear chains ($M_w \sim 1.21 \times 10^7$ g mol^{-1}) at 15 °C and different x. Similar to PS discussed in Fig. 1, at $x < 1$, there exists only a single peak related to translational diffusion. As x increases further, the first peak becomes broader and shifts to larger Γ/q^2 because the observation length scale ($1/q$) is much smaller than R_g, and more internal motions with larger Γ contribute to the relaxation and mix with the translational diffusion in $S(q,t)$. Finally, two peaks merge into one broader peak and the diffusion motion and internal motion can no longer be separated.

Fig. 5 shows a plot of $\Gamma_{peak2}/(Dq^2)$ against x, where Γ_{peak2} is the average line width of the second peak in Fig. 4. Experimental data for polystyrene in toluene at 20 °C previously mentioned (Fig. 2) are also shown in Fig. 5. It is clearly to see that the two plots follow a similar pattern. The dotted lines in Fig. 5 show the predicted $[1 + \Gamma_n/(Dq^2)]$ dependence on x for polystyrene in toluene. Similar to the tendency of PS in good solvent toluene, the data for PNIPAM in water respectively follow the dotted lines of $n = 1$ in $3 < x < 6$; $n = 2$ in $3 < x < 6$; $n = 3$ in $6 < x < 10$; and $n = 4$ in $10 < x < 15$. The analysis stops when $x > 15$ because of the difficulty in separating the two peaks. Again, the estimation of the Γ_1 to Γ_4 agrees well with the previous result, revealing that internal motions associated with $2\Gamma_n$, *i.e.*, $\Gamma_n + \Gamma_n$, dominates the relaxations measured in dynamic LLS in different ranges of x. We suggested that some energetically favored internal motion at the certain range of x could not be detected by the dynamic LLS, resulting in this discrepancy between the experimental result and theoretical prediction.

As discussed above, the employed PNIPAM chains can undergo a coil-to-globule transition in response to external stimuli by temperature. One might therefore wonder how the internal motions are suppressed when the chains are shrinking. To answer this question, internal motions of PNIPAM chains at different solution temperatures are investigated. Fig. 6 shows that the extrapolation of the time-average scattered light intensity at different solution temperatures to the zero angle leads to an identical value, *i.e.*, there is no change in the weight-average molar mass, but the scattered light intensity becomes much less dependent on the scattering angle as the solution temperature increases. On the basis of eqn (14), Fig. 6 clearly reveals the collapse of individual chains as the solution temperature

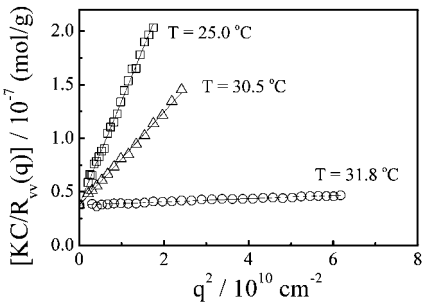

Fig. 6 Scattering-vector (angular) dependent time-average scattered light intensity (Rayleigh ratio) of poly(*N*-isopropylacrylamide) linear chains in water at three different temperatures. Reprinted with permission from ref. 60 (2010 American Chemical Society).

increases with no interchain association. Otherwise, we would see an increase of the scattered light intensity at $q = 0$ because the scattered light intensity is proportional to the square of the mass of a scattering object. Fig. 6 lays a solid ground for us to study the internal motions of individual chains at different solution temperatures, especially under the Θ and poor solvent conditions.[60] On the other hand, Fig. 7 summarizes how the average sizes of individual polymer chains vary with the solution temperature, where the dash line marks the Θ temperature and the poor solvent region is on its right side. A comparison of the chain sizes under the good (lower temperatures) and the poor (higher temperatures) solvent conditions reveals that individual chains do not shrink too much up to the Θ temperature and the collapse of individual PNIPAM chains occur within a very narrow temperature window after passing the Θ point. Fig. 7 enables us to calculate our experimentally reachable range of $x = (qR_g)^2$ at each solution temperature.

Fig. 8 shows how the Dq^2-scaled line-width distribution changes with the solution temperature for a given scattering angle. It is important to point out that here it is the change of $<R_g>$ that varies x; and $1/q \sim 54$ nm. The second peak related to the internal motions becomes smaller and smaller as the solution temperature increases. It is clear to see that as the solution temperature increases beyond the Θ temperature (~30.5 °C), each chain in water dramatically shrinks and x decreases from 21.5 to 0.37 within the range 30.5–33.0 °C. In their fully collapsed state ($T \sim 33.0$ °C, $<R_g> \sim 27$ nm and $x < 1$), there is only one diffusive relation and no internal motions appear. On the other

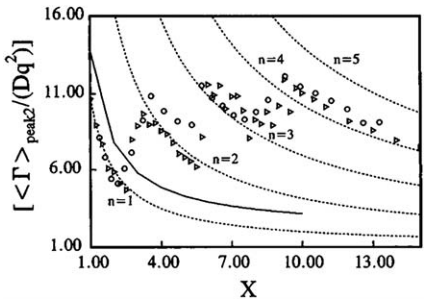

Fig. 5 Plots of the reduced average line-width $\Gamma_{peak2}/(Dq^2)$ *versus* x. (○) PNIPAM linear chain in water at $T = 15.0$ °C; (△) polystyrene in toluene at $T = 20.0$ °C. The dashed line are predicated on Zimm's non-draining model. Reprinted with permission from ref. 35 (1995 American Chemical Society).

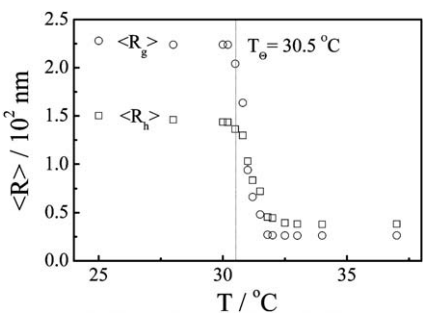

Fig. 7 Solution-temperature dependent average radius of gyration and hydrodynamic radius of poly(*N*-isopropylacrylamide) linear chains in water. Reprinted with permission from ref. 60 (2010 American Chemical Society).

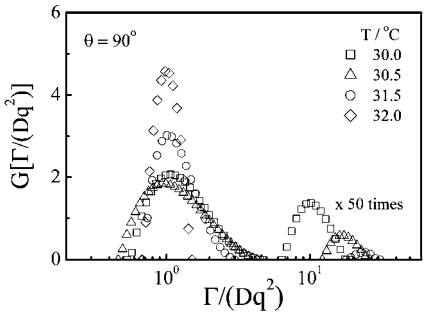

Fig. 8 Solution-temperature dependent line-width distributions $G[\Gamma/(Dq^2)]$ of poly(*N*-isopropylacrylamide) linear chains in water, where the peak related to internal motions is enlarged by a factor of 50 times for a better view. Reprinted with permission from ref. 60 (2010 American Chemical Society).

hand, the decrease of the peak area (the contribution of the internal motions to the line-width distribution) reflects the suppression of internal motions as each chain shrinks. To our knowledge, there has been no theory about such a decrease yet, but it is physically reasonable; namely, as the chain collapses, it becomes more and more difficult for the thermal energy (k_BT) to excite its internal motions.

To study it more quantitatively, we evaluate how the contribution of internal motion changes during the transition process. Fig. 9, shows the weighting (the ratio of the two peaks) of the internal motion at different scattering angles varies with temperature. In the good solvent region, $A_I/(A_I + A_D)$ essentially remains a constant for each given scattering angle, revealing that the slight shrinking of individual chains in this region has no effect on its internal motions because each chain still remains a random-coil conformation. When the solvent quality becomes poorer, $A_I/(A_I + A_D)$ dramatically drops and the internal motions disappear at temperatures higher than ~32 °C at which the chain collapsed. Surprisingly, at different scattering angles, $A_I/(A_I + A_D)$ always turns near the Θ temperature. Again, there is no theory to predict such a turning point, but it is physically reasonable. Namely, polymer chains are agitated by the thermal energy, to undergo the internal motions they have to overcome the entropic force in a good solvent because of the chain swelling and the segment-segment interaction (enthalpy) in a poor solvent. At its "ideal" state, the entropic cost is balanced by the enthalpy interaction.

To further illustrate why the internal motions of linear PNIPAM chains disappear at higher temperatures, we plot the temperature dependence of the ratio of the average radius of gyration to the average hydrodynamic radius, as shown in Fig. 10. $\langle R_g\rangle/\langle R_h\rangle$ is a parameter that describes the chain conformation. For linear flexible chains in good solvent and hard spheres with a uniform density, both theoretical and experimental studies have showed that $\langle R_g\rangle/\langle R_h\rangle \sim 1.5$ and ~ 0.77, respectively.[33] As expected, the change of $\langle R_g\rangle/\langle R_h\rangle$ would follow the dashed line in Fig. 10 and approach 0.77 when the chain is fully collapsed. However, we have consistently observed a dip (minimum) of $\langle R_g\rangle/\langle R_h\rangle$ before the chain reaches its globular state. Such a dip is related to the so-called molten globular state in which many small loops are formed on the periphery of a shrunk chain, as schematically shown in Fig. 10. These small loops lead to a larger hydrodynamic size, but have little effect on the radius of gyration because of their insignificant masses, so that $\langle R_g\rangle/\langle R_h\rangle < 0.774$ predicted for a uniform non-draining sphere. A combination of Fig. 9 and 10 clearly reveal that the internal motions are still visible when $\langle R_g\rangle/\langle R_h\rangle$ is still in the dip but disappears after it reaches the plateau, supporting our previously proposed concept of the molten globular state.[58]

2.4 Internal motions of spherical PNIPAM microgels in dilute solution

Microgel particle is a cross-linked latex particle which is swollen by a good solvent. PNIPAM microgels have attracted a lot of attention due to its swollen to shrunk transition accompanied with temperature change. Saunders and coworkers demonstrated that a delicate balance between interactions favoring swelling of microgel particles exists (*e.g.* salvation of the PNIPAM chains *via* hydrogen bonding with water) and those responsible for collapse (*e.g.* inter and intra-chain hydrogen bonding and elasticity of the network).[61] Utilizing the dynamic LLS, our group followed the variation of internal motion with the change of solvent quality.

Fig. 11 shows how PNIPAM spherical microgel particles shrink with increasing temperature. A comparison of Fig. 7 and 11 shows that the microgels collapse much less than the chains, presumably due to the cross-linking that already prevents the

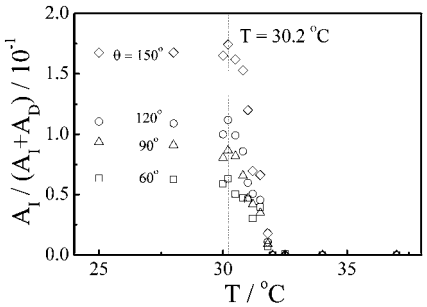

Fig. 9 Solution-temperature dependent area ratio $A_I/(A_I + A_D)$ of two peaks, respectively, related to internal motions and diffusion of poly(*N*-isopropyl-acrylamide) linear chains in water at different scattering angles, where the dashed line marks the point at which internal motions are completely suppressed. Reprinted with permission from ref. 60 (2010 American Chemical Society).

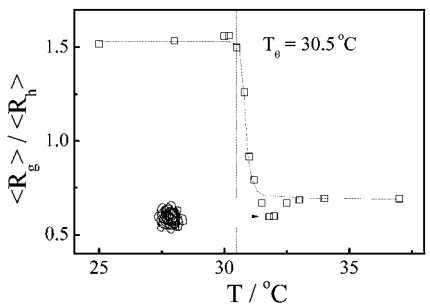

Fig. 10 Solution-temperature dependent ratio of average radius of gyration and hydrodynamic radius of poly(*N*-isopropylacrylamide) linear chains in water, where the dash line marks the Θ temperature, and the arrow points to the molten globule state, which is schematically shown on the left. Reprinted with permission from ref. 60 (2010 American Chemical Society).

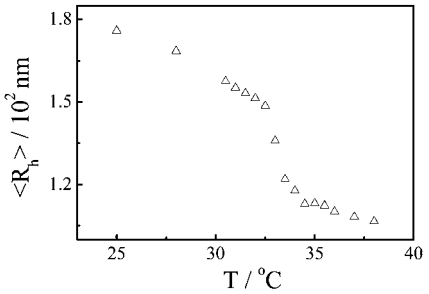

Fig. 11 Dispersion-temperature dependent average hydrodynamic radius of poly(*N*-isopropylacrylamide) spherical microgels in in water. Reprinted with permission from ref. 60 (2010 American Chemical Society).

swollen of the gel network at lower temperatures. In addition, Fig. 12 shows that in contrast to linear chains where internal motions were observed at $x \sim 1$, the second peak related with the internal motions of the microgels is much weak and appears only when $x \geq 8$ at 25.0 °C; namely, we can only observe their internal motions when $1/q \sim 50$ nm $\leq <R_g>/3$, instead of at $1/q \sim <R_g>$, implying that the thermal energy can excite the entire linear chain with its longest normal mode, but only a small portion of a gel network with a dimension of ~50 nm. If imaging that the gel network is made of small uniform meshes with a dimension of ~10 nm on the basis of the cross-linking density, we are able to estimate that the internal motions only involve about $\sim 10^2$ of such meshes from the minimum $1/q$. Note that such measured internal motions are slower than the relaxation of the subchains ("blobs") of a macroscopic gel network with a similar cross-linking density, but faster than the translational diffusion of individual microgels in dispersion.

Fig. 13 reveals that $A_I/(A_I + A_D)$ initially increases as the microgels shrink in the good solvent region, reflecting the increase of the average chain density with the temperature. Further increase of the temperature leads to a more and quick collapse of the microgels as well as a sharp decrease of $A_I/(A_I + A_D)$, starting at 32.5 °C that is two degrees higher than the Θ temperature of PNIPAM linear chains in water. At 37 °C, the microgel approaches their fully collapsed state and $A_I/(A_I + A_D)$ becomes zero, indicating complete suppression of the internal motions. The increase of $A_I/(A_I + A_D)$ can be attributed to

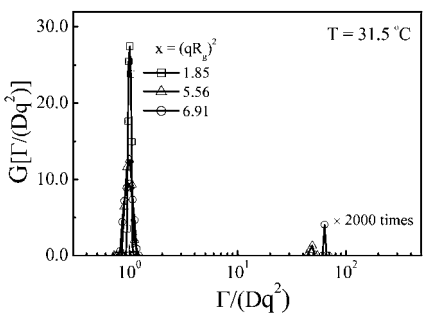

Fig. 12 *x*-dependent q^2-scaled line-width distributions $G[\Gamma/(Dq^2)]$ of poly(*N*-isopropylacrylamide) spherical microgels in water, where the peak related to internal motions is enlarged by a factor of 2,000 times for a better view. Reprinted with permission from ref. 60 (2010 American Chemical Society).

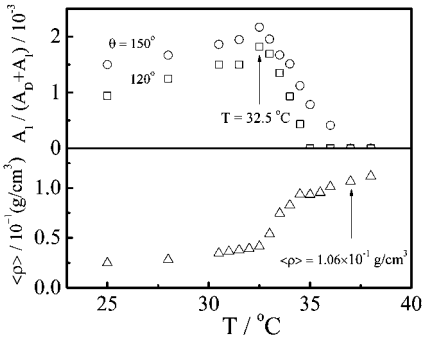

Fig. 13 Dispersion-temperature dependent average chain density ($<\rho>_{chain}$) defined in terms of its hydrodynamic volume, and area ratio $A_I/(A_I + A_D)$ of two peaks, respectively, related to internal motions and diffusion of poly(*N*-isopropylacrylamide) spherical microgels in water at two different scattering angles, where the dashed line marks the temperature at which internal motions become the strongest and the arrow points to the density when internal motions are completely suppressed. Reprinted with permission from ref. 60 (2010 American Chemical Society).

a gradual decrease of the entropic elasticity (elastic module) of the gel network because the microgel becomes "softer" when it swells less as the dispersion approaches its Θ temperature.

Following our previous argument that a polymer chain should be most deformable at its ideal state; namely, the interaction among its segments is balanced by that between solvent and segment, we can mark this turning point of $A_I/(A_I + A_D)$ as the Θ temperature of the PNIPAM microgels in water. It has been known that the volume phase transition of a gel network, depending on whether it has a lower or upper critical solution temperature (LCST or UCST), shifts to a higher or lower temperature as the cross-linking density increases, *i.e.*, the average length of the sub-chains between two neighboring cross-linking points decreases.[59] For a PNIPAM gel network in water with a LCST, the shift of its Θ temperature from 30.5 °C to 32.5 °C is reasonable.[34]

3. Conclusion

The dynamics of flexible polymer chains in dilute solution, in particular the internal motions for flexible linear polystyrene (PS) and polyisoprene (PIP) chain in both good and Θ solvent is reviewed. It has been found that the first and second relaxation time can be deduced using dynamic LLS, with the values closed to the prediction of non-draining Zimm model. Moreover, the relaxation time of the flexible polymer chains mainly depends on the nature of chain dynamics in different solvents. To interpretate the dynamic structure using first cumulant, generally speaking, the trend of $\eta_0\Omega(q)/k_BTq^3$ dependence on qR_g, that is q^2 dependence for $qR_g \ll 1$ and q^3 dependence for $qR_g \gg 1$, is consistent with the description of non-draining model and reflects the flexible nature of the polymer chains. The trend has been confirmed by experiments but the predicted plateau value is always higher than those from experiments. Such a discrepancy should lead to a revision of classical theory and construction of new models and explanations. More factors like internal friction and hydrodynamic screening are suggested to be included in the

model, while other speculations, such as the defect in detecting some energetically favored internal motion by dynamic LLS are also proposed.

In the past fifteen years, our group studied the internal motions of temperature sensitive polymer, poly(*N*-isopropylacrylamide), including both chains and microgels. In good solvent, we observe the internal motion at $1/q \sim R_g$ for linear chain and $1/q \sim R_g/3$ for microgel, indicating that the thermal energy (k_BT) is able to excite the entire linear chain but only part of the microgel network with a dimension of ~50 nm to undergo the longest normal mode. The first cumulant study of both linear chains and microgels lead to the finding that the internal motions associated with $2\Gamma_n$ dominate the relaxation mode in dynamic LLS in different x ranges. This discovery hints that some energetically favorable internal mode may not be detected by dynamic LLS in the specific x range.

As the solvent quality changes from Θ to bad, the intensity of internal motions weakens gradually due to the coil-to-globule transition of linear chain or sub-chains inside the microgel network, indicating overlapping of the chain suppresses the internal motion in the semi and concentrated regions. We also found that the contribution from internal motions makes a turning around the Θ temperature, presumably due to the interaction among chain segments and among solvent molecules and segments are balanced. This finding may lead a more convenient way to estimate the Θ temperature of polymer solution.

Acknowledgements

The financial support of Ministry of Science and Technology of China (2007CB936401), the National Natural Scientific Foundation of China (NNSFC) Projects (20934005 and 50773077) and the Hong Kong Special Administration Region Earmarked Project (CUHK4039/08P, 2160361; CUHK4028/09P, 2160387) is gratefully acknowledged.

References

1 P. E. Rouse, *J. Chem. Phys.*, 1953, **21**, 1271–1280.
2 B. Zimm, *J. Chem. Phys.*, 1956, **24**, 269–278.
3 R. Pecora, *J. Chem. Phys.*, 1968, **49**, 1032–1035.
4 B. Chu, *Polym. J.*, 1985, **17**, 225–238.
5 P. G. de Gennes, *Physics*, 1967, **3**, 37–45.
6 C. Han and A. Akcasu, *Macromolecules*, 1981, **14**, 1080–1084.
7 I. Teraoka, *Polymer Solution: An Introduction to Physical Properties*, John Wiley & Sons, Inc, New York, 2002.
8 O. Kramer and J. E. Frederic., *Macromolecules*, 1972, **5**, 69–75.
9 J. Mcadam, T. King and A. Knox, *Chem. Phys. Lett.*, 1973, **19**, 351–354.
10 J. Mcadam and T. King, *Chem. Phys.*, 1974, **6**, 109–116.
11 J. Mcadam and T. King, *Chem. Phys. Lett.*, 1974, **28**, 90–92.
12 C. C. Han, *Rev. Sci. Instrum.*, 1978, **49**, 31–38.
13 E. Dubois-Violette and P. G. de Gennes, *Physics*, 1967, **3**, 181–198.
14 B. Chu, *Laser Light Scattering*, Acdemic Press, New York, 1974.
15 B. J. Berne and R. Percora, *Dynamic Light Scattering*, Wiley, New York, 1976.
16 R. Pecora, *Dynamic Light Scattering: Application of Photon Correlation Spectroscopy*, Plenum Press, New York, 1985.
17 S. Provencher, *Makromol. Chem., Macromol. Chem. Phys.*, 1979, **180**, 201–209.
18 G. Jones and D. Caroline, *Chem. Phys.*, 1979, **40**, 153–156.
19 E. Gulari, E. Gulari, Y. Tsunashima and B. Chu, *J. Chem. Phys.*, 1979, **70**, 3965–3972.
20 S. Kim, D. Ramsay, G. Patterson and J. Selser, *J. Polym. Sci., Part B: Polym. Phys.*, 1990, **28**, 2023–2056.
21 K. Venkataswamy, A. Jamieson and R. Petschek, *Macromolecules*, 1986, **19**, 124–133.
22 G. Meyerhoff and B. Appelt, *Macromolecules*, 1979, **12**, 968–971.
23 G. Schulz and H. Baumann, *Makromol. Chem., Macromol. Chem. Phys.*, 1968, **114**, 122–138.
24 B. Appelt and G. Meyerhoff, *Macromolecules*, 1980, **13**, 657–662.
25 H. Utiyama, S. Utsumi, Y. Tsunashima and M. Kurata, *Macromolecules*, 1978, **11**, 506–514.
26 Y. Miyaki, Y. Einaga and H. Fujita, *Macromolecules*, 1978, **11**, 1180–1186.
27 M. Adam and M. Delsanti, *Macromolecules*, 1977, **10**, 1229–1237.
28 M. Fukuda, M. Fukutomi, Y. Kato and T. Hashimoto., *J. Polym. Sci., Polym. Phys. Ed.*, 1974, **12**, 871–890.
29 K. Yamaguchi, A. Hirao, K. Suzuki, K. Takenaka, S. nakahama and N. Yamazaki, *J. Polym. Sci., Polym. Lett. Ed.*, 1983, **21**, 395–401.
30 N. Sawatari, T. Yoshizaki and H. Yamakawa, *Macromolecules*, 1998, **31**, 4218–4222.
31 V. Boyko, S. Richter, W. Burchard and K. Arndt, *Langmuir*, 2007, **23**, 776–784.
32 Y. Tsunashima, M. Hirata, N. Nemoto, K. Kajiwara and M. Kurata, *Macromolecules*, 1987, **20**, 2862–2866.
33 C. Wu and X. Wang, *Phys. Rev. Lett.*, 1998, **80**, 4092–4094.
34 H. Senff and W. Richtering, *J. Chem. Phys.*, 1999, **111**, 1705–1711.
35 C. Wu and S. Zhou, *Macromolecules*, 1996, **29**, 1574–1578.
36 M. Benmouna and A. Akcasu, *Macromolecules*, 1978, **11**, 1187–1192.
37 A. Akcasu, M. Benmouna and C. Han, *Polymer*, 1980, **21**, 866–890.
38 W. Burchard, M. Schmidt and W. Stockmayer, *Macromolecules*, 1980, **13**, 580–587.
39 M. Bixon and R. Zwanzig, *J. Chem. Phys.*, 1978, **68**, 1890–1895.
40 R. Pecora, *J. Chem. Phys.*, 1965, **43**, 1562–1564.
41 A. Perico, P. Piaggio and C. Cuniberti, *J. Chem. Phys.*, 1975, **62**, 2690–2695.
42 A. Perico, P. Piaggio and C. Cuniberti, *J. Chem. Phys.*, 1975, **62**, 4911–4918.
43 Z. Akcasu and H. Gurol, *J. Polym. Sci., Polym. Phys. Ed.*, 1976, 1–10.
44 P. Wiltzius and D. Cannell, *Phys. Rev. Lett.*, 1986, **56**, 61–64.
45 Y. Tsunashima, N. nemoto and M. Kurata, *Macromolecules*, 1983, **16**, 1184–1188.
46 N. Nemoto, Y. Makita, Y. Tsunashima and M. Kurata, *Macromolecules*, 1984, **17**, 425–430.
47 Y. Tsunashima, N. Nemoto and M. Kurata, *Macromolecules*, 1983, **16**, 584–589.
48 A. Livesey, P. Licinio and M. Delaye, *J. Chem. Phys.*, 1986, **84**, 5102–5107.
49 W. Huang and J. E. Frederic., *Macromolecules*, 1974, **7**, 34–39.
50 T. King and M. Treadaway, *J. Chem. Soc., Faraday Trans. 2*, 1976, **72**, 1473–1481.
51 M. Adam and M. Delsanti, *J. Phys., Lett.*, 1977, **38**, L271–L273.
52 G. Jones and D. Caroline, *Chem. Phys.*, 1979, **37**, 187–194.
53 M. Bhatt and A. Jamieson, *Macromolecules*, 1989, **22**, 2724–2730.
54 B. Chu, Z. Wang and J. Yu, *Macromolecules*, 1991, **24**, 6832–6838.
55 C. Wu, K. Chan and K. Xia, *Macromolecules*, 1995, **28**, 1032–1037.
56 M. Bhatt and A. Jamieson, *Macromolecules*, 1988, **21**, 3015–3022.
57 M. Kurata, Y. Tsunashima, M. Iwama and K. Kamada, *Polymer Handbook*, Wiley, New York, 1975.
58 C. Wu and S. Zhou, *Phys. Rev. Lett.*, 1996, **77**, 3053–3055.
59 K. Dusek and D. Patterso., *J. Polym. Sci., Part A-2*, 1968, **6**, 1209–1216.
60 Z. Dai and C. Wu, *Macromolecules*, 2010, **43**, 10064–10070.
61 B. Saunders, H. Crowther, G. Morris, S. Mears, T. Cosgrove and B. Vincent, *Colloids Surf., A*, 1999, **149**, 57–64.